Paper

Performance Analysis of Filtered OFDM Based Downlink and Uplink NOMA System over Nakagami-*m* Fading Channel

Shaika Mukhtar and Gh. Rasool Begh

National Institute of Technology (NIT) Srinagar, Jammu and Kashmir, India

https://doi.org/10.26636/jtit.2021.148020

Abstract—Efficient consumption of available resources and fulfillment of increasing demands are the two main challenges which are addressed by exploring advanced multiple access schemes along with efficient modulation techniques. To this end, non-orthogonal multiple access (NOMA) is discussed as a promising scheme for future 5G traffic. NOMA enables the users to share same resource block, permitting certain level of interference. In this paper, we propose filtered OFDM (F-OFDM) as a transmission waveform for NOMA systems, as it offers all the advantages of OFDM with the additional provision of sub-band filtering to satisfy the diverse services of the users. We examine F-OFDM in both downlink and uplink NOMA systems. Error-related performances of both downlink and uplink F-OFDM NOMA systems are analyzed and compared with conventional OFDM NOMA system over Nakagami-*m* fading channel. The results show that the error performance of F-OFDM NOMA is better than that of OFDM NOMA. An improvement of about 2 dB and 1 dB in bit error rate is achieved in downlink and uplink F-OFDM NOMA, respectively. Monte Carlo simulations are conducted for different values of fading parameter *m*, supporting the obtained analytical results.

Keywords—bit error rate, orthogonal multiple access, out-of-band emission, successive interference cancellation.

1. Introduction

The 5G era is envisioned to consist of huge number of users, requiring low latency and high speed connectivity. To support such a scenario, there has been an evolution in the manner of sharing limited resources among the users [1]. The traditional orthogonal multiple access (OMA) schemes, such as TDMA, ensure absolute orthogonality among the users, leading to negligible inter-user interference [2]. This level of non-interference helps in easy extraction of message signals at the receiver. However, these OMA schemes are not sufficiently capable of supporting large number of users because of the limited availability of resources. To overcome this hurdle, the idea of non-orthogonal multiple access has been introduced [3], [4], wherein users share their resources. In NOMA, freedom degrees (time, frequency, code) are exploited in a non-orthogonal manner, using superposition coding that leads to a certain level of interference among the users. To overcome the effect of this interference, successive interference cancellation (SIC) is used at the receiver. Non-orthogonal resource sharing in NOMA offers diverse advantages, for example improved spectral efficiency and throughput, unbiased fairness among the users, reduction in user scheduling, and reduction in latency [3]. These useful features of NOMA motivate the incorporation of NOMA in future communication systems. To improve the performance of NOMA, the choice of waveform is a critical issue. Orthogonal frequency division multiplexing is one of the well-known waveform designs for NOMA. However, OFDM suffers from high peak to average power ratio (PAPR) and out-of-band emission (OOBE) [6], [7]. Larger out-of-band emissions occur due to disturbing transitions from one block to another. Such an undesirable feature causes interference to adjacent channel users [8], [9]. One simple way of reducing OOBE in OFDM is to shape the transmitting signal properly, in order to achieve better spectral confinement.

In this paper, we exploit the idea of the sub-band filtering of OFDM waveform, leading to the generation of an F-OFDM waveform. In a multiuser scenario, such sub-band splitting and filtering is beneficial, as optimized numerology may be used to satisfy service diversity-related requirements in 5G networks [9], [10]. In addition to the advantages of the foundational OFDM waveform, F-OFDM alleviates the use of the guard band, providing better spectral efficiency. It is also MIMO-friendly, ensuring higher compatibility with other technologies as well [11]. Based on all these desirable features, F-OFDM evolves as a suitable choice for NOMA systems.

2. Literature Review

Over the past few years, NOMA has been extensively studied worldwide. In [5], a unified network for NOMA

transmission has been described and its standardization has been presented. Considering the choice of waveforms for NOMA, the OFDM NOMA model is proposed in [6], with the different issues affecting this approach addressed. In [9], the authors compared each of the available 5G waveforms with F-OFDM and concluded that F-OFDM is a promising waveform for 5G. As far as service diversity is concerned, [10] analyzes OFDM-based waveforms in the presence of mixed numerologies, and concludes that F-OFDM shows better spectral performance and robustness than other OFDM-based waveforms. In [12], various pulse shaping filter designs for filtered OFDM are discussed, wherein semiequiripple filter, equiripple filter and windowed sinc filters are analyzed.

In [13], the authors have proposed generalized fast convolution-based filtered OFDM, wherein highly selective sub-band filtering is performed. Being simpler in concept, F-OFDM is gaining attention in low latency based 5G communication, as discussed in [14], where the authors analyzed a polar coded filtered OFDM system. In [15], SINR analysis of OFDM and F-OFDM for machine type communications are researched, with the authors observing that F-OFDM has a potential to mitigate undesirable distortions leading to better SINR results. For asynchronous uplink 5G communications, the usefulness of F-OFDM is considered in [16] and, accordingly, closed form expressions are derived for intercarrier interference (ICI).

3. Research Contribution

Based on the available literature regarding NOMA, we observe that the incorporation of F-OFDM in NOMA system has not been discussed yet. Considering this research gap, we propose to explore the utility of F-OFDM in the NOMA system.

In this paper, OFDM NOMA signals are spectrally shaped by using a sinc filter and Hann windowing. Actually, the impulse response of the sinc filter stretches to infinity on both ends. To exploit the advantages of the sinc filter used as a pulse shaping filter, truncation of impulse response is carried out using window functions [9]. The basic idea behind windowing is to obtain the product of the impulse response of filter $h(t)$ and window function $w(t)$:

$$H_w(t) = h(t).w(t) \ . \tag{1}$$

This soft truncation leads to better impulse response of the pulse shaping filter, ensuring lower inter symbol interference (ISI). These specifically designed filters are efficient enough to balance between frequency and time localization [17]. The effect of applying pulse shaping and windowing is shown in Fig. 1, where the power spectral densities of OFDM and F-OFDM are compared. It is evident that the filter has shaped a basic OFDM signal so that the gain of 80 dB is achieved in side lobe attenuation. This improvement of spectral characteristics is reflected in the constellation diagram of the F-OFDM NOMA signal, as shown in Fig. 2. Upon comparing the constellation diagram of the F-OFDM NOMA signal with the constellation

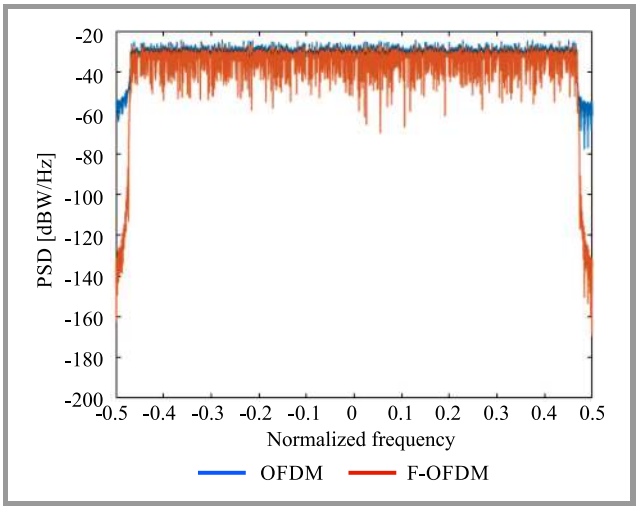

Fig. 1. Power spectral density comparison of OFDM and F-OFDM.

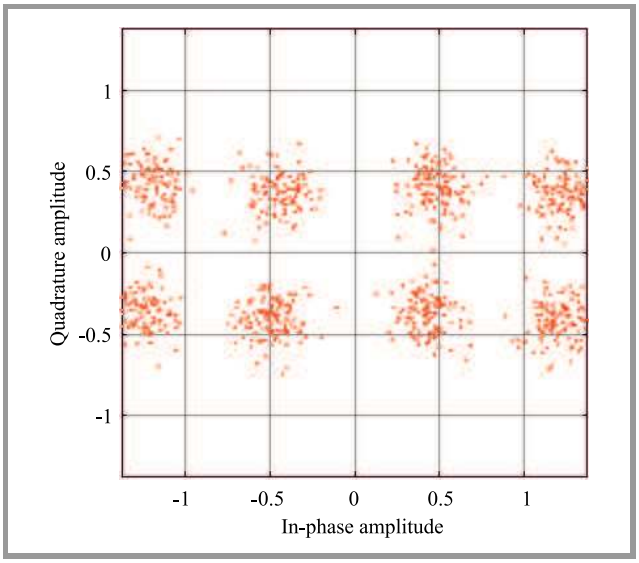

Fig. 2. Constellation diagram of F-OFDM NOMA signal.

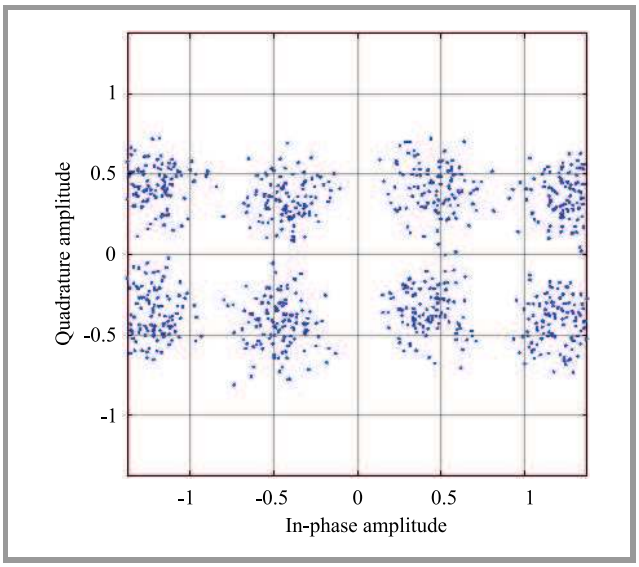

Fig. 3. Constellation diagram OFDM NOMA signals.

diagram of a simple OFDM-NOMA signal shown in Fig. 3, it is obvious that F-OFDM constellation points are more concentrated than OFDM signal points, due to better SNR. To the best of our knowledge, this is the first paper which considers BER performance of F-OFDM based downlink and uplink NOMA systems. We also consider the generic Nakagami-m fading channel to analyze the behavior of the system, as this model presents both strong and weak fading scenarios by altering the value of fading parameter m [18]. The main contributions of this paper are:

- We propose Filtered OFDM based downlink and uplink NOMA models with windowed sinc filters for spectral shaping.
- We derive and examine the exact closed form BER expressions of downlink Filtered OFDM NOMA users over Nakagami-*m* fading channel.
- For uplink mode, the analysis usually becomes intractable, so we derive and analyze approximate closed form BER expressions of uplink Filtered OFDM NOMA users over Nakagami-*m* fading channel.
- The derived expressions are presented in compact form which are easily implementable in common software packages. The obtained simulations for different values of fading parameter m support the validity of these derived analytical expressions.

The rest of the paper is organized as follows. Section 4 describes the architecture of the proposed downlink and uplink F-OFDM NOMA system. BER performance assessment of the proposed downlink and uplink F-OFDM NOMA models is shown in Sections 5 and 6, respectively. The obtained results are simulated and discussed in Section 7, with conclusions presented in Section 8.

4. F-OFDM NOMA System Model

First, we consider the downlink F-OFDM NOMA system consisting of a base station (BS) and two users – near user (NUE) and far user (FUE). We assume that the channel conditions of NUE are better than those of FUE. So, QPSK modulation is used for NUE and BPSK modulation is used for FUE to achieve better spectral efficiency [4]. After modulation, the modulated signals are multiplied by their respective allotted power levels such that symbol energies are $E_{NUE} = \alpha P_s$ and $E_{FUE} = (1-\alpha)P_s$ with α being the power coefficient and P_s being the total transmit power. Depending on channel conditions, more power is allotted to the far user than the near user, keeping the total transmitted power equal to a unity. This step ensures user fairness in the NOMA system. After this fractional transmit power allocation (FTPA), the signals are superposed [6]. The generated superimposed signal is given by:

$$x = \sqrt{E_{NUE}}x_{NUE} + \sqrt{E_{FUE}}x_{FUE} \ , \tag{2}$$

where x_{NUE} and x_{FUE} are QPSK and BPSK modulated signals of NUE and FUE, respectively. The signal given by Eq. (2) is fed to the IFFT block to generate OFDM symbols s_{ofdm}. A cyclic prefix is appended to s_{ofdm} to mitigate the effect of ISI. The OFDM signal generated in this manner undergoes pulse shaping by passing through a low pass filter $f(n)$. We realize this low pass filter by considering sinc filter as a pulse shaping filter, truncated using the Hann window. These soft truncated filters have a sharp transition band to reduce guard bands [14]. The output of the filter is given as:

$$s_f = s_{ofdm} * f(n) \ , \tag{3}$$

where '$*$' represents the convolution operation. This F-OFDM signal is transmitted by the BS. The signals received at NUE and FUE, after passing through their respective AWGN channels, are:

$$\begin{aligned} y_{NUE} &= s_f + w_{NUE} \ , \\ y_{FUE} &= s_f + w_{FUE} \ , \end{aligned} \tag{4}$$

where w_{NUE} and w_{FUE} represent AWGN noise (zero mean, $N_0/2$ variance) of NUE and FUE channels, respectively.
At FUE receiver, the received signal y_{FUE} is first passed through the matched filter $f^*(-n)$, which maximizes the SNR of the received signal and avoids interference from neighboring users [17]. After this, the cyclic prefix is removed and FFT operation is carried out. Then, BPSK demodulation provides the message signal of FUE. No SIC is performed at FUE, leading to a simpler receiver. On the other hand, the decoding process at NUE involves execution of SIC. NUE first decodes the FUE signal. Then, SIC block eliminates interference caused by the far user signal. After removal of far user symbols, NUE decodes its own message signal.
Furthermore, the proposed uplink FOFDM NOMA model is described in the following manner. The transmitter side of uplink F-OFDM NOMA consists of two users which are communicating with the BS. The near user (NUE) modulates its signal and feeds its QPSK modulated signal to the IFFT block to generate OFDM symbols to which a cyclic prefix (CP) is appended. After this, pulse shape filtering and windowing is performed, leading to the formation of F-OFDM signal of NUE, x_{nue}, which is transmitted to BS. Simultaneously, FUE generates and transmits its F-OFDM signal x_{fue}. These NUE and FUE F-OFDM signals are received at BS with different SNRs, depending on their respective transmit power and channel conditions [19]. The BS performs all the decoding in the uplink scenario. The signal received at the BS using uplink F-OFDM NOMA is given as:

$$y = \sqrt{P_N}\,x_{nue} + \sqrt{P_F}\,x_{fue} + w \ , \tag{5}$$

where P_N and P_F are transmit power levels of NUE and FUE, respectively, and w is AWGN noise. BS first performs SIC and decodes the NUE signal. After subtraction of NUE signals from the received signal, the remaining signal is used to decode FUE signals. In this way, message signals of both users are decoded by BS [20].

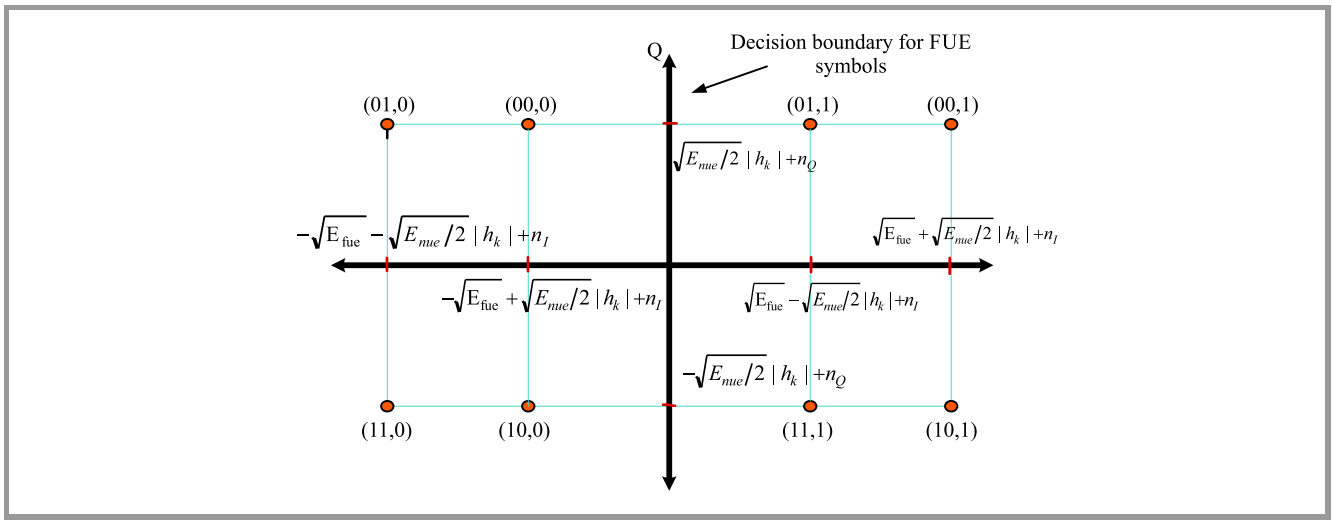

Fig. 4. Signal space representation of superposed F-OFDM signal received by users in the downlink mode.

5. Performance Evaluation of Downlink F-OFDM NOMA

We derive the BER expressions of F-OFDM based NOMA users over Nakagami-*m* fading channel. We incorporate the filter block acting as a spectrum shaper with the spectrum shaping factor p. As described in the model, at each user, the received signal, after passing through the matched filter and the OFDM demodulator, is sent to the decoder block. In the downlink mode, the signal space received by both users (NUE and FUE) is shown in Fig. 4.

Here, the superposed symbols are represented in the form of (y_1, y_2, y_3) with y_1 and y_2 bits representing the first and the second bit of QPSK modulated NUE symbols, and y_3 representing BPSK modulated bits of FUE. The decision logic is based on the concept that an error in any superposed symbol may occur, when the in-phase AWGN noise is strong enough to shift the received symbol to another region across the decision boundary [21]. The decoding is done using the maximum likelihood (ML) detector over the superposed symbols. The probability of error is given by the sum of the probability of error of each symbol multiplied by their respective prior probabilities [23]. Here, prior probabilities of all superposed symbols are assumed to be equal.

5.1. Error probability of Downlink Filtered Far User

Here, we consider the decoding of FUE symbols by taking NUE symbols as noise. Using ML detection at FUE, we have [22]:

$$P_{fue}(e) = \frac{1}{2}P\left(n_I \geq \sqrt{E_{fue}} + \sqrt{E_{nue}/2}\right) + \frac{1}{2}P\left(n_I \geq \sqrt{E_{fue}} - \sqrt{E_{nue}/2}\right) . \quad (6)$$

Here, $E_{fue} = p.E_{FUE}$ and $E_{nue} = p.E_{NUE}$, where p is the shaping factor which depends on the properties of the designed filter (as shown in Appendix B). Also, E_{fue} and E_{nue} are respective filtered symbol energies of the far and near NOMA user. In terms of Gaussian Q function, we have:

$$P_{fue}(e) = \frac{1}{2}\left[Q(\sqrt{\gamma_1}) + Q(\sqrt{\gamma_2})\right] , \quad (7)$$

where γ_1 and γ_2 represent filtered SNRs of outer four and inner four constellation points of the signal space diagram given in Fig. 4:

$$\gamma_1 = \left(\sqrt{\frac{2E_{fue}}{N_o}} + \sqrt{\frac{E_{nue}}{N_o}}\right)^2 ,$$
$$\gamma_2 = \left(\sqrt{\frac{2E_{fue}}{N_o}} - \sqrt{\frac{E_{nue}}{N_o}}\right)^2 . \quad (8)$$

Equation 7 gives the expression for instantaneous error probability of F-OFDM modulated downlink FUE NOMA user in AWGN channel. Now, we consider the fading environment which leads to the inclusion of channel coefficients in the derivation of BER expressions:

$$P_{fue}(e) = \frac{1}{2}\left[Q(\sqrt{\gamma_3}) + Q(\sqrt{\gamma_4})\right] , \quad (9)$$

where γ_3 and γ_4 represent faded SNRs of outer four and inner four constellation points from Fig. 4, where:

$$\gamma_3 = \left(\sqrt{\frac{2E_{fue}}{N_o}} + \sqrt{\frac{E_{nue}}{N_o}}\right)^2 |h_{fue}|^2 ,$$
$$\gamma_4 = \left(\sqrt{\frac{2E_{fue}}{N_o}} - \sqrt{\frac{E_{nue}}{N_o}}\right)^2 |h_{fue}|^2 . \quad (10)$$

Evaluating the average BER over fading channel:

$$\overline{P_{fue}(e)} = \frac{1}{2}\left[\underbrace{\int_0^\infty Q(\sqrt{\gamma_3})\, f_{\gamma_3}(\gamma_3)\mathrm{d}\gamma_3}_{I_3} + \underbrace{\int_0^\infty Q(\sqrt{\gamma_4})\, f_{\gamma_4}(\gamma_4)\mathrm{d}\gamma_4}_{I_4}\right] . \quad (11)$$

Considering Nakagami-*m* fading distribution, the integrals I_3 and I_4 are given by [24]:

$$I_3 = \frac{1}{2}\left[1 - \sqrt{\frac{\frac{\overline{\gamma_3}}{2}}{m+\frac{\overline{\gamma_3}}{2}}}\sum_{k=0}^{m-1}\binom{2k}{k}\left(\frac{1-\frac{\frac{\overline{\gamma_3}}{2}}{m+\frac{\overline{\gamma_3}}{2}}}{4}\right)^k\right],$$

$$I_4 = \frac{1}{2}\left[1 - \sqrt{\frac{\frac{\overline{\gamma_4}}{2}}{m+\frac{\overline{\gamma_4}}{2}}}\sum_{k=0}^{m-1}\binom{2k}{k}\left(\frac{1-\frac{\frac{\overline{\gamma_4}}{2}}{m+\frac{\overline{\gamma_4}}{2}}}{4}\right)^k\right], \quad (12)$$

where m is fading parameter ranging from 0.5 to ∞ and:

$$\overline{\gamma_3} = \left(\sqrt{\frac{2E_{fue}}{N_o}} + \sqrt{\frac{E_{nue}}{N_o}}\right)^2 E\left[|h_{fue}|^2\right],$$

$$\overline{\gamma_4} = \left(\sqrt{\frac{2E_{fue}}{N_o}} - \sqrt{\frac{E_{nue}}{N_o}}\right)^2 E\left[|h_{fue}|^2\right]. \quad (13)$$

On substituting Eq. (12) in Eq. (11), we have:

$$\overline{P_{fue}(e)} = \frac{1}{4}\left[1 - \sqrt{\frac{\frac{\overline{\gamma_3}}{2}}{m+\frac{\overline{\gamma_3}}{2}}}\sum_{k=0}^{m-1}\binom{2k}{k}\left(\frac{1-\frac{\frac{\overline{\gamma_3}}{2}}{m+\frac{\overline{\gamma_3}}{2}}}{4}\right)^k\right] + \frac{1}{4}\left[1 - \sqrt{\frac{\frac{\overline{\gamma_4}}{2}}{m+\frac{\overline{\gamma_4}}{2}}}\sum_{k=0}^{m-1}\binom{2k}{k}\left(\frac{1-\frac{\frac{\overline{\gamma_4}}{2}}{m+\frac{\overline{\gamma_4}}{2}}}{4}\right)^k\right]. \quad (14)$$

Hence, Eq. (14) gives the average error probability of spectrally shaped OFDM downlink FUE over the Nakagami-*m* fading channel for integer values of *m*. On substituting *m*=1 in Eq. (14), we obtain the average probability of error for FUE over the Rayleigh fading channel, which is given by:

$$\overline{P_{fue}(e)} = \frac{1}{4}\left[\left(1 - \sqrt{\frac{\frac{\overline{\gamma_3}}{2}}{m+\frac{\overline{\gamma_3}}{2}}}\right) + \left(1 - \sqrt{\frac{\frac{\overline{\gamma_4}}{2}}{m+\frac{\overline{\gamma_4}}{2}}}\right)\right]. \quad (15)$$

The closed form average BER expressions given in Eqs. (14)–(15) are compact presenting the behavior of downlink FUE over Nakagami-*m* and Rayleigh fading channels, respectively.

5.2. Error Probability of Downlink Filtered Near User

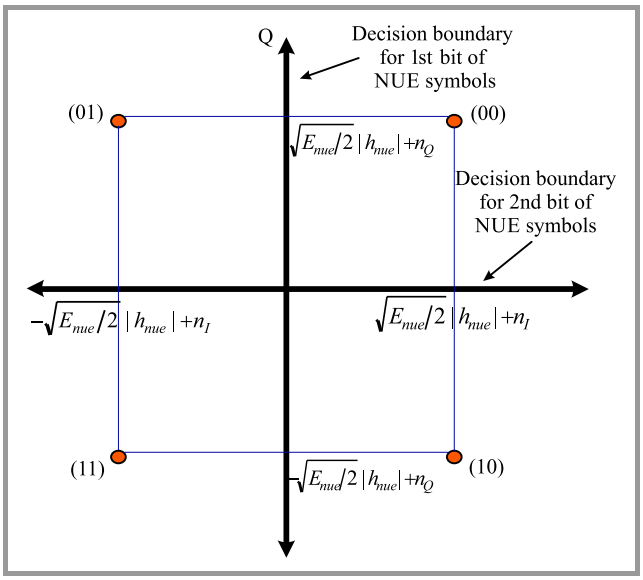

Fig. 5. Signal space representation after correct decoding and subtraction of filtered FUE symbols.

The detection of NUE symbols depends on the correct detection of FUE symbols. The signal space remaining after correct detection and subtraction of FUE symbols is given in Fig. 5. Here, the prior probabilities given by Eq. (6) are used to calculate the error probability of NUE. Considering ML detection, the probability of error of NUE symbols is obtained by taking the average of error probabilities of two bits [22]. Using [21] along with our proposed pulse shaping of the transmitting signals, we have:

$$P_{nue} = \frac{1}{4}\left[Q(\sqrt{\gamma_5}) \times \{4 - Q(\sqrt{\gamma_6}) - Q(\sqrt{\gamma_7})\} - Q(\sqrt{\gamma_6})\right], \quad (16)$$

where the filtered SNRs are given as:

$$\gamma_5 = \frac{E_{nue}}{N_o}|h_{nue}|^2,$$

$$\gamma_6 = \left(\sqrt{\frac{2E_{fue}}{N_o}} + \sqrt{\frac{E_{nue}}{N_o}}\right)^2 |h_{nue}|^2,$$

$$\gamma_7 = \left(\sqrt{\frac{2E_{fue}}{N_o}} - \sqrt{\frac{E_{nue}}{N_o}}\right)^2 |h_{nue}|^2. \quad (17)$$

Now, for evaluating average BER over the Nakagami-*m* fading channel, we solve each Q-function term of Eq. (16) in the similar manner as we solved Eq. (9) for FUE in the downlink mode. After the results so obtained are substituted in Eq. (16), we have:

$$\overline{P_{nue}(e)} = \frac{1}{8}\left[P_5 \times \{8 - P_6 - P_7\} - P_6\right] \ , \qquad (18)$$

with

$$P_5 = 1 - \sqrt{\frac{\frac{\overline{\gamma_5}}{2}}{m+\frac{\overline{\gamma_5}}{2}}} \sum_{k=0}^{m-1} \binom{2k}{k} \left(\frac{1-\frac{\frac{\overline{\gamma_5}}{2}}{m+\frac{\overline{\gamma_5}}{2}}}{4}\right)^k ,$$

$$P_6 = 1 - \sqrt{\frac{\frac{\overline{\gamma_6}}{2}}{m+\frac{\overline{\gamma_6}}{2}}} \sum_{k=0}^{m-1} \binom{2k}{k} \left(\frac{1-\frac{\frac{\overline{\gamma_6}}{2}}{m+\frac{\overline{\gamma_6}}{2}}}{4}\right)^k ,$$

$$P_7 = 1 - \sqrt{\frac{\frac{\overline{\gamma_7}}{2}}{m+\frac{\overline{\gamma_7}}{2}}} \sum_{k=0}^{m-1} \binom{2k}{k} \left(\frac{1-\frac{\frac{\overline{\gamma_7}}{2}}{m+\frac{\overline{\gamma_7}}{2}}}{4}\right)^k , \qquad (19)$$

and

$$\overline{\gamma_5} = \frac{E_{nue}}{N_o} E\left[|h_{nue}|^2\right] \ ,$$

$$\overline{\gamma_6} = \left(\sqrt{\frac{2E_{fue}}{N_o}} + \sqrt{\frac{E_{nue}}{N_o}}\right)^2 E\left[|h_{nue}|^2\right] \ ,$$

$$\overline{\gamma_7} = \left(\sqrt{\frac{2E_{fue}}{N_o}} - \sqrt{\frac{E_{nue}}{N_o}}\right)^2 E\left[|h_{nue}|^2\right] \ . \qquad (20)$$

In this way, Eq. (18) gives the average probability of error of NUE in a downlink F-OFDM NOMA system over the Nakagami-*m* fading channel for integer values of *m*. On substituting *m*=1 in Eq. (18), we obtain error probability of NUE over the Rayleigh channel.

6. Performance Evaluation of Uplink F-OFDM NOMA

In the uplink mode, the signal space of the received signal at BS is shown in Fig. 6. The received signal is a combination of user signals and noise. In the uplink mode, BS performs SIC to decode NUE signals and then, after subtraction, FUE signals are decoded. In this way, the decoding order in the uplink mode is the reverse of the process in the downlink F-OFDM NOMA [19].

6.1. Error Probability of Uplink Filtered Near User

Assuming that x_{NUE} and x_{FUE} symbols have equal prior probabilities and using the concept of ML detection presented in Eq. (6), the probability of a NUE error is given as [21]:

$$P_{nue}(e) = \frac{1}{2}P\left(n_Q \geq \sqrt{E_{nue}/2}h_{nue}\right) + \frac{1}{4}\left\{P\left(n_I \geq \sqrt{E_{nue}/2}h_{nue} + \sqrt{E_{fue}/2}h_{fue}\right) + P\left(n_I \geq \sqrt{E_{nue}/2}h_{nue} - \sqrt{E_{fue}/2}h_{fue}\right)\right\} . \qquad (21)$$

A simplified form of the equation is:

$$P_{nue}(e) = \frac{1}{2}\left[Q(\sqrt{\gamma_8}) + \frac{1}{2}Q(u) + \frac{1}{2}Q(v)\right] \ , \qquad (22)$$

where:

$$\gamma_8 = \frac{E_{nue}}{N_o}|h_{nue}|^2 \ ,$$

$$u = \sqrt{\frac{E_{nue}}{N_o}}h_{nue} + \sqrt{\frac{2E_{fue}}{N_o}}h_{fue} \ ,$$

$$v = \sqrt{\frac{E_{nue}}{N_o}}h_{nue} - \sqrt{\frac{2E_{fue}}{N_o}}h_{fue} \ . \qquad (23)$$

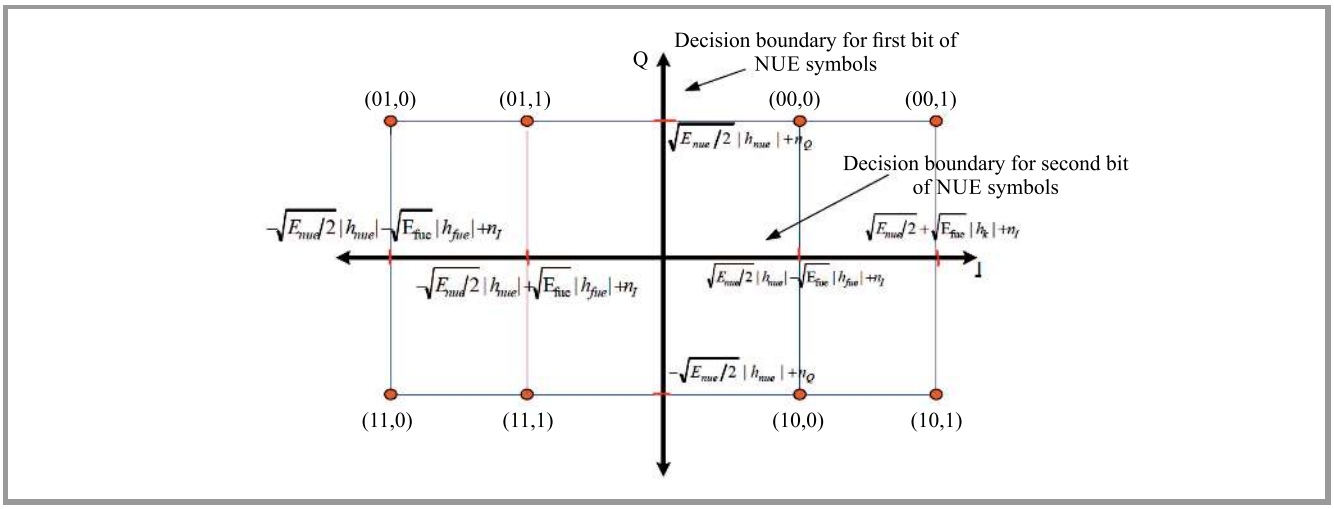

Fig. 6. Signal space representation of the received signal at BS in uplink F-OFDM NOMA.

Here, variables u and v represent the sum of and the difference between two random variables, respectively. We assume that two users in uplink NOMA transmit independently and face the same type of fading channel. So, we consider the sum of and the difference between two independent and identical distributed random variables (h_{nue} and h_{fue}). Further, we know that the value of Gaussian Q function of the sum of two quantities is lower than the difference between the same quantities. Considering this fact, we have $Q(u) << Q(v)$. Ignoring the sum term, the error probability of F-OFDM modulated NUE in the uplink mode is:

$$P_{nue}(e) = \frac{1}{2}\left[Q(\sqrt{\gamma_8}) + \frac{1}{2}Q(v)\right] . \tag{24}$$

Evaluating average BER over the fading channel, we have:

$$\overline{P_{nue}(e)} = \frac{1}{2}\left[\underbrace{\int_0^\infty Q(\sqrt{\gamma_8}) f_{\gamma_8}(\gamma_8)\mathrm{d}\gamma_8}_{I_8} + \frac{1}{2}\underbrace{\int_0^\infty Q(v) f(v)\mathrm{d}v}_{I_v}\right] . \tag{25}$$

The integrals in Eq. (25) can be easily implemented in common software packages, but considering the need of having compact expressions, we derive approximate closed-form average BER expressions in terms of well-known functions, such as Beta and Gauss hypergeometric functions.

Integral I_8 is one of the integrals of Eq. (25) which is easily solved by following the analytical steps performed in the downlink scenario for the Nakagami-*m* fading channel:

$$I_8 = \frac{1}{2}\left[1 - \sqrt{\frac{\frac{\overline{\gamma_8}}{2}}{m+\frac{\overline{\gamma_8}}{2}}}\sum_{k=0}^{m-1}\binom{2k}{k}\left(\frac{1-\frac{\frac{\overline{\gamma_8}}{2}}{m+\frac{\overline{\gamma_8}}{2}}}{4}\right)^k\right] , \tag{26}$$

where:

$$\overline{\gamma_8} = \frac{E_{nue}}{N_o}E[|h_{nue}|^2] . \tag{27}$$

Now, by considering the fact that h_{nue} and h_{fue} are independent, integral I_v may be rewritten as [21]:

$$I_v = \int_0^\infty\int_0^\infty Q\left(a_1 h_{nue} - a_2 h_{fue}\right) f_{h_{nue}}(h_{nue}) f_{h_{fue}}(h_{fue})\mathrm{d}h_{nue}\mathrm{d}h_{fue} , \tag{28}$$

where:

$$a_1 = \sqrt{E_{nue}/N_o} , \quad a_2 = \sqrt{2E_{fue}/N_o} . \tag{29}$$

We solve integral I_v by considering Chernoff bound of Q function [26]:

$$Q(x) \cong \frac{1}{2}\mathrm{e}^{\frac{x^2}{2}} . \tag{30}$$

This approximation simplifies the analysis over fading channels, so we have:

$$I_v \cong \int_0^\infty\int_0^\infty \mathrm{e}^{\frac{(a_1 h_{nue} - a_2 h_{fue})^2}{2}} f_{h_{nue}}(h_{nue}) f_{h_{fue}}(h_{fue})\mathrm{d}h_{nue}\mathrm{d}h_{fue} \tag{31}$$

After solving this integral as shown in Appendix A, we have:

$$I_v \cong N\times\left[\frac{B(2m,\frac{1}{2})}{(a_1a_2)^{2m}}{}^2F_1(m,m+0.5;2m+0.5;0.5-2G) + \frac{\Gamma(m+0.5)\sqrt{\pi}}{\Gamma(m)}\frac{a_1a_2}{(AC)^{m+0.5}}{}^2F_1(m+0.5,m+0.5;1.5;\frac{K}{C})\right] , \tag{32}$$

where $B(.,.)$ and ${}^2F_1(.,.;.;.)$ are Beta and Gauss hypergeometric functions given in [25]. Here:

$$N = \frac{4}{(\Gamma m)^2}\left(\frac{m}{\Omega}\right)^{2m}\frac{\Gamma 2m}{2^{2m}},\ G = \frac{E}{F^2},\ E = \left(\frac{a_2^2}{2}+\frac{m}{\Omega}\right) - \frac{a_1^2a_2^2}{8A},\ F = \frac{a_1a_2}{\sqrt{2A}},\ A = \left(\frac{a_1^2}{2}+\frac{m}{\Omega}\right),\ K = \frac{a_1^2a_2^2}{4A}, C = \left(\frac{a_2^2}{2}+\frac{m}{\Omega}\right) . \tag{33}$$

Using Eq. (26) and Eq. (32) in Eq. (25), we have:

$$\overline{P_{nue}(e)} = \frac{1}{4}\left\{\left[1 - \sqrt{\frac{\frac{\overline{\gamma_8}}{2}}{m+\frac{\overline{\gamma_8}}{2}}}\sum_{k=0}^{m-1}\binom{2k}{k}\left(\frac{1-\frac{\frac{\overline{\gamma_8}}{2}}{m+\frac{\overline{\gamma_8}}{2}}}{4}\right)^k\right] + N\times\left[\frac{B(2m,\frac{1}{2})}{(a_1a_2)^{2m}}{}^2F_1(m,m+0.5;2m+0.5;0.5-2G)\right] + \frac{\Gamma(m+0.5)\sqrt{\pi}}{\Gamma(m)}\frac{Na_1a_2}{(AC)^{m+0.5}} {}^2F_1\left(m+0.5,m+0.5;1.5;\frac{K}{C}\right)\right\} . \tag{34}$$

This is an expression of the approximate error probability of NUE in the uplink scenario over the Nakagami-*m* fading channel, in terms of Beta and Gauss hypergeometric functions, for integer values of m. Furthermore, the error probability of NUE in the uplink scenario over the Rayleigh fading channel is obtained by substituting $m = 1$ in Eq. (34) leading to:

$$\overline{P_{nue}(e)} = \frac{1}{4}\left[1-\sqrt{\frac{\overline{\gamma_8}}{2+\overline{\gamma_8}}}\right] + \frac{1}{4\Omega^2}\left[\frac{B(2,0.5)}{(a_1a_2)^2} \times {}^2F_1\left(1,1.5;2.5;0.5-2Z\right) + \frac{\Gamma(1.5)\sqrt{\pi}a_1a_2}{4(PQ)^{1.5}}\left(1-\frac{Y}{Q}\right)^{-1.5}\right], \quad (35)$$

where:

$$Z=\frac{R}{S^2},\ R=\left(\frac{a_2^2}{2}+\frac{1}{\Omega}\right)-\frac{a_1^2a_2^2}{8P}, F=\frac{a_1a_2}{\sqrt{2P}},$$
$$P=\left(\frac{a_1^2}{2}+\frac{1}{\Omega}\right),\ Y=\frac{a_1^2a_2^2}{4P},\ Q=\left(\frac{a_2^2}{2}+\frac{1}{\Omega}\right). \quad (36)$$

We observe that the derived approximate average BER expressions over Nakagami-*m* and Rayleigh fading channels are described by well-known functions which are usually used in wireless communication. These functions are readily available in common software packages which help in providing better comparison with the simulations.

6.2. Error Probability of Uplink Filtered Far User

After decoding NUE symbols, BS subtracts these symbols from the main signal and performs decoding of FUE symbols. The signal space representation after subtraction of decoded NUE symbols is shown in Fig. 7. Error probabilities of each symbol within the constellation may be calculated by considering the decision boundary [21]:

$$P_{fue}(e) = \frac{1}{2}P\left(\sqrt{E_{fue}}h_{fue} \le n_I \le \sqrt{E_{nue}/2}h_{nue} + \sqrt{E_{fue}h_{fue}}\right) + \frac{1}{2}P\left(n_I \le -\sqrt{E_{fue}}\right). \quad (37)$$

In terms of Q function, we have:

$$P_{fue}(e) = Q\left(\sqrt{\gamma_9}\right) - \frac{1}{2}Q(u), \quad (38)$$

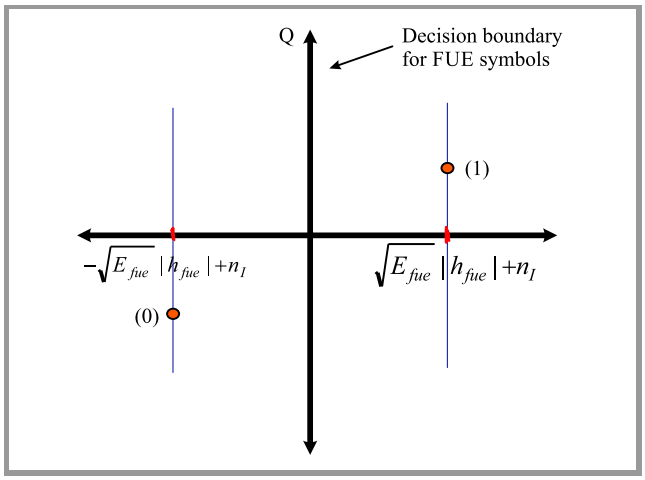

Fig. 7. Representation of signal space remaining at BS after subtraction of correctly decoded NUE symbols.

where:

$$\gamma_9 = \frac{2E_{fue}}{N_o}|h_{fue}|^2, \qquad \overline{\gamma_9} = \frac{2E_{fue}}{N_o}E[|h_{fue}|^2],$$
$$u = a_1h_{nue} + a_2h_{fue}\ . \quad (39)$$

For average probability of error of uplink FUE over fading channel:

$$\overline{P_{fue}(e)} = \underbrace{\int_0^\infty Q\left(\sqrt{\gamma_9}\right)f_{\gamma_9}(\gamma_9)\mathrm{d}\gamma_9}_{I_9} - \frac{1}{2}\underbrace{\int_0^\infty Q(u)f(u)\mathrm{d}u}_{I_u}. \quad (40)$$

Using the Nakagami-*m* fading model analysis [22]:

$$I_9 = \frac{1}{2}\left[1-\sqrt{\frac{\frac{\overline{\gamma_9}}{2}}{m+\frac{\overline{\gamma_9}}{2}}}\sum_{k=0}^{m-1}\binom{2k}{k}\left(\frac{1-\frac{\frac{\overline{\gamma_9}}{2}}{m+\frac{\overline{\gamma_9}}{2}}}{4}\right)^k\right]. \quad (41)$$

Integral I_u is given by:

$$I_u = \int_0^\infty Q(u)f(u)\mathrm{d}u\ . \quad (42)$$

For the Nakagami-*m* fading environment, integral I_u is solved similarly to integral I_v for uplink NUE. Following the manipulations shown in Appendix A, we have:

$$I_u \cong N\times\left[\frac{B(2m,\frac{1}{2})}{(a_1a_2)^{2m}}{}^2F_1\left(m,m+0.5;2m+0.5;0.5-2G\right)\right]. \quad (43)$$

Upon substituting the expressions of I_9 and I_u given by Eq. (41) and Eq. (43), respectively, in Eq. (40):

$$\overline{P_{fue}(e)} = \frac{1}{2}\left[1-\sqrt{\frac{\frac{\overline{\gamma_9}}{2}}{m+\frac{\overline{\gamma_9}}{2}}}\sum_{k=0}^{m-1}\binom{2k}{k}\left(\frac{1-\frac{\frac{\overline{\gamma_9}}{2}}{m+\frac{\overline{\gamma_9}}{2}}}{4}\right)^k\right] - \frac{1}{2}\left[N\times\frac{B(2m,\frac{1}{2})}{(a_1a_2)^{2m}}{}^2F_1\left(m,m+0.5;2m+0.5;0.5-2G\right)\right]. \quad (44)$$

For the Rayleigh fading channel, we take $m=1$ in Eq. (44):

$$\overline{P_{fue}(e)} = \frac{1}{2}\left[1-\sqrt{\frac{\overline{\gamma_9}}{2+\overline{\gamma_9}}}\right] - \frac{1}{2\Omega^2}\left[\frac{B(2,0.5)}{(a_1a_2)^2}{}^2F_1\left(1,1.5;2.5;0.5-2Z\right)\right]. \quad (45)$$

The approximate closed-form BER expressions for FUE in the uplink mode, derived with the use of the proposed model are described by well-known functions. Such compact expressions help to follow the dependence of BER on different fading parameters.

7. Results and Discussions

We simulate the proposed F-OFDM NOMA model using MATLAB software. We consider the following simulation parameters:

- IFFT/FFT points = 1024,
- cyclic prefix length = 64,
- filter length = 513,
- sinc filter – prototype,
- Hann windowing.

For spectrum shaping, the length of the sinc filter is assumed to equal 513, which is greater than the cyclic prefix, thus leading to better OOBE reduction [17]. F-OFDM ensures 80 dB suppression in side lobe power, resulting in lower OOBE. This helps mitigate interference between adjacent users. Hence, we propose F-OFDM as a better modulation technique for NOMA systems. While simulating the obtained analytical results, we take pulse shaping factor of $p = 1.5$ (see Appendix B), considering moderate SNR improvement achieved by using the simulated pulse shaping filter.

7.1. Performance of Downlink F-OFDM NOMA

We evaluate BER performance of both NOMA user types in AWGN, as well as Rayleigh and Nakagami-*m* channels, using the proposed downlink F-OFDM NOMA model. The power coefficients assigned to NUE and FUE in the downlink mode are 0.2 and 0.8, respectively. Monte Carlo simulations are performed to observe variations in BER with SNR changes. The curves so obtained are plotted, such that the solid lines represent the analytical results obtained and the line markers (*) represent the simulation results.

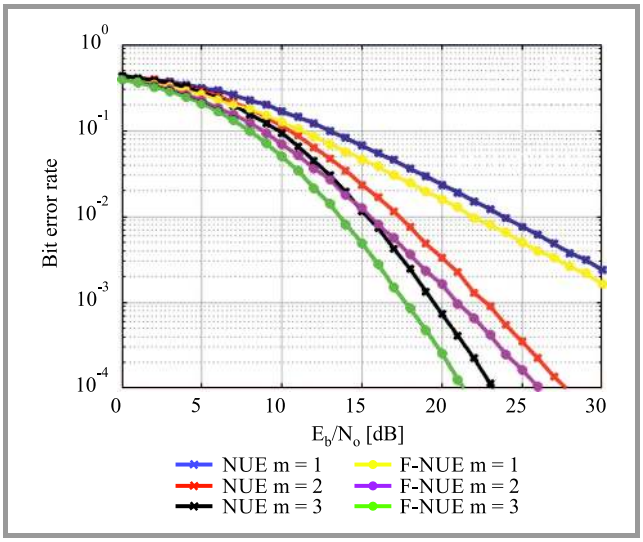

Fig. 9. BER performance of NUE in downlink F-OFDM NOMA over the Nakagami-*m* channel.

Interpretation of the curves shows that the proposed spectrally shaped NUE and FUE offer better performance in all three channels (AWGN, Rayleigh and Nakagami-*m*), with a considerable BER improvement of approximately 2 dB. Such an improvement is quite motivating to implement F-OFDM in downlink NOMA. We observe that fading leads to higher BERs, as is visible from Rayleigh BER curves in Figs. 8 and 10. Furthermore, over the Nakagami-*m* fading channel, user behaviors for different values of *m* (1, 2, and 3) are observed and shown in Figs. 9 and 11. It is evident that an increase in fading parameter *m* leads to

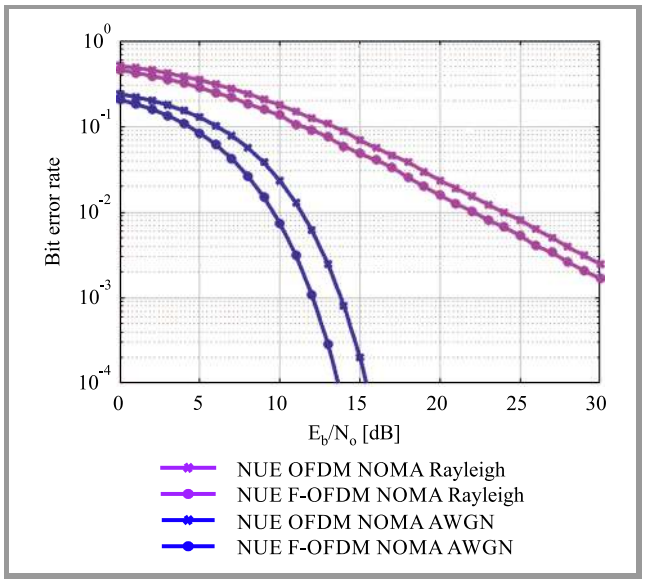

Fig. 8. BER performance of NUE in downlink F-OFDM NOMA in AWGN and over the Rayleigh channel.

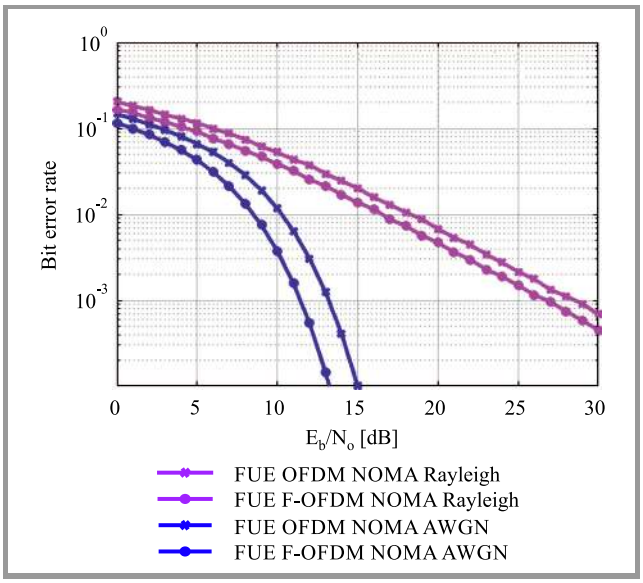

Fig. 10. BER performance of FUE in downlink F-OFDM NOMA in AWGN and over the Rayleigh channel.

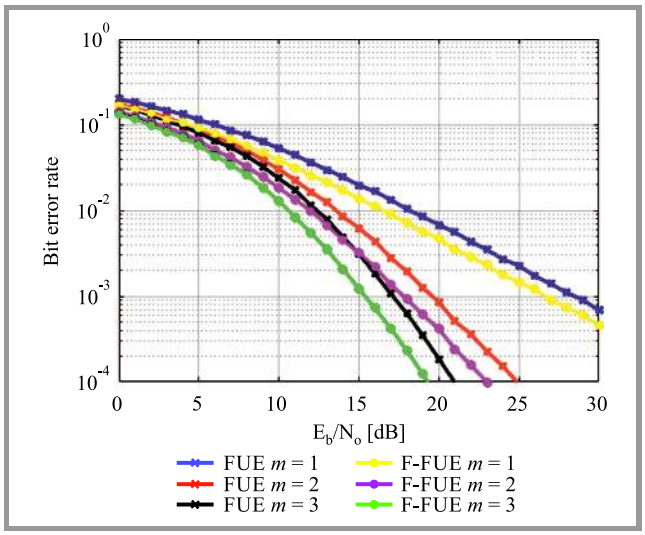

Fig. 11. BER performance of FUE in downlink F-OFDM NOMA over the Nakagami-*m* channel.

better BER performance. This is attributed to the fact that higher *m* means lower fading leading to better BER results [24].

7.2. Performance of Uplink F-OFDM NOMA

In the proposed uplink F-OFDM NOMA, we evaluate BER performance of both NUE and FUE in AWGN, Rayleigh and Nakagami-*m* channels. The simulations are plotted to present differences between BER and SNR. It is observed from the BER curves that the proposed spectrally shaped NUE and FUE show better performance in AWGN, Rayleigh and Nakagami-*m* channels, with a BER improvement of approximately 1 dB. Such a BER improvement is lower than in the proposed downlink F-OFDM NOMA.

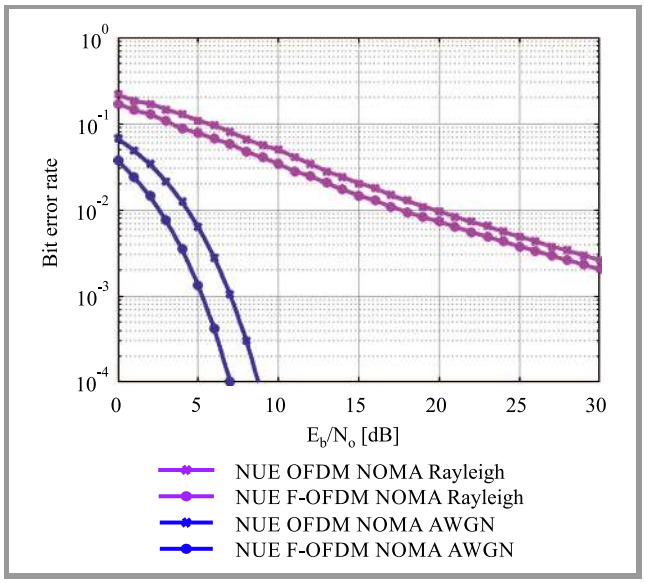

Fig. 12. The BER performance of NUE in uplink F-OFDM NOMA in AWGN and Rayleigh channel.

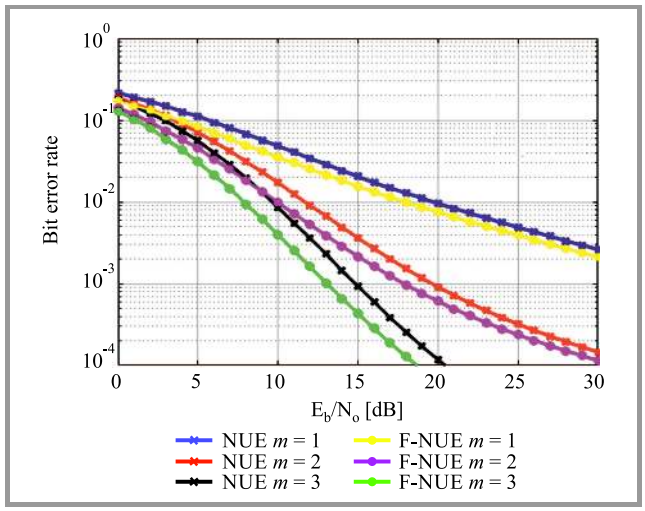

Fig. 13. The BER performance of NUE in uplink F-OFDM NOMA over Nakagami-*m* channel.

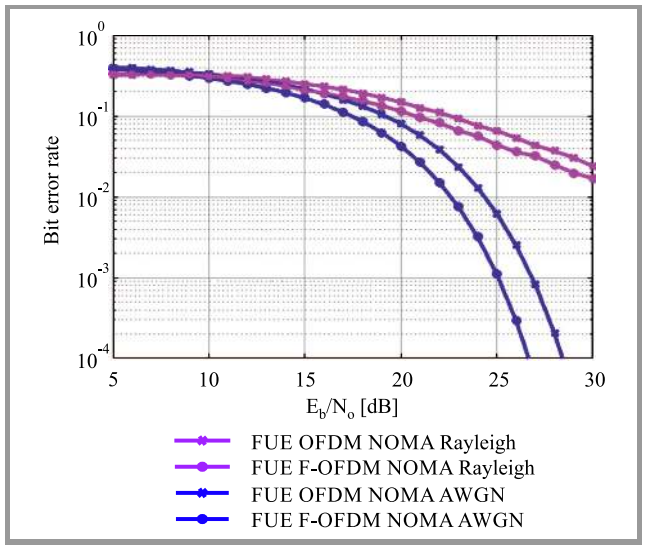

Fig. 14. The BER performance of FUE in uplink F-OFDM NOMA in AWGN and Rayleigh channel.

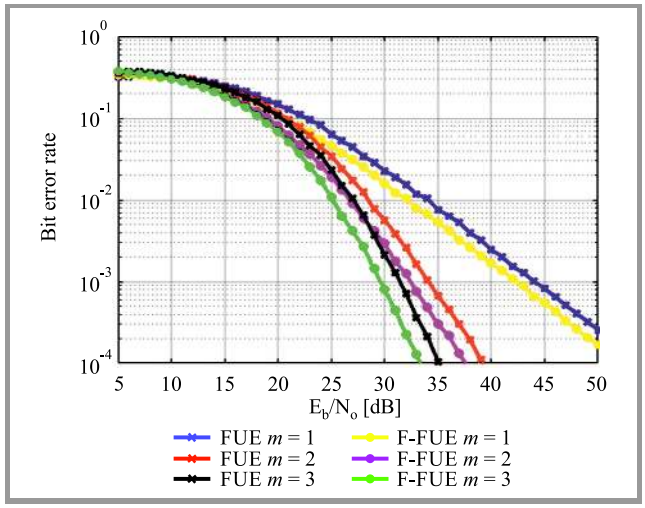

Fig. 15. The BER performance of FUE in uplink F-OFDM NOMA over Nakagami-*m* channel.

Just as in the downlink scenario, Rayleigh curves show higher BER than AWGN curves, as shown in Figs. 12 and 14. Furthermore, we observe the user behaviors over the Nakagami-*m* channel for different values of *m* (1, 2, and 3), as shown in Figs. 13 and 15. It is evident that BER decreases with an increase in *m*, following the behavior shown by the users in the downlink mode over the Nakagami-*m* fading channel.

8. Conclusions

NOMA is a promising multiple access technique capable of meeting the diverse needs of the increasing number of users. Selection of an efficient modulation technique determines the performance of the NOMA system. In this paper, we propose the use of filtered OFDM as an efficient modulation technique for NOMA. F-OFDM has the potential to support the diverse nature of services rendered in NOMA environments. In this paper, simple sinc filtering along with Hann windowing is performed to generate F-OFDM NOMA signals characterized by better spectral confinement. We evaluate the performance of F-OFDM based downlink and uplink NOMA systems. For the downlink scenario, we derive compact, closed-form BER expressions of near and far NOMA users over the Nakagami-*m* fading channel. For the uplink mode, we derive approximate BER expressions for both users, described by easily implementable functions, over the Nakagami-*m* fading channel. Monte Carlo simulations are carried out to validate the analytical results obtained. Simulations are performed for different values of fading parameter *m*. Using the proposed model, BER improvement of nearly 2 dB and 1 dB is achieved by NOMA users in the downlink and uplink scenarios, respectively. Such behavior of F-OFDM NOMA encourages the application of F-OFDM in NOMA systems intended for 5G.

Appendix A

Integral I_v is given by:

$$I_v \cong \int_0^{\infty} [I_{inner1}]\, \mathrm{e}^{-\frac{a_2^2 h_{fue}^2}{2}} f_{h_{fue}}(h_{fue}) \mathrm{d}h_{fue} \ , \qquad (46)$$

where I_{inner1} is:

$$I_{inner1} = \int_0^{\infty} \mathrm{e}^{-\frac{a_1^2 h_{nue}^2}{2}} \mathrm{e}^{a_1 a_2 h_{nue} h_{fue}} f_{h_{nue}}(h_{nue}) \mathrm{d}h_{nue} \ . \qquad (47)$$

I_{inner1} is solved by considering Nakagami-*m* distribution with *m* as fading parameter and $\Omega = E[|h_{nue}|^2]$:

$$I_{inner1} = \frac{2}{\Gamma m} \left(\frac{m}{\Omega}\right)^m \int_0^{\infty} \mathrm{e}^{-A h_{nue}^2 + M h_{nue}} h_{nue}^{2m-1} \mathrm{d}h_{nue} \ , \qquad (48)$$

where:

$$A = \frac{a_1^2}{2} + \frac{m}{\Omega}, \quad M = a_1 a_2 h_{fue} \ . \qquad (49)$$

Using the standard solution given in [25], the solution of Eq. (48) is given as:

$$I_{inner1} = \frac{2}{\Gamma m} \left(\frac{m}{\Omega}\right)^m \frac{\Gamma 2m}{(2A)^m} \mathrm{e}^{\frac{M^2}{8A}} D_{-2m} \frac{-M}{\sqrt{2A}} \ , \qquad (50)$$

where $D_v(.)$ is the parabolic cylinder function [25]. Substituting the expression for $D_v(-z)$ given in [28] in Eq. (50):

$$I_{inner1} = I_x + I_y \ , \qquad (51)$$

where:

$$I_x = \frac{2}{\Gamma m} \left(\frac{m}{\Omega}\right)^m \frac{\Gamma 2m}{(2A)^m} \mathrm{e}^{\frac{M^2}{8A}} D_{-2m} \left(\frac{M}{\sqrt{2A}}\right),$$

$$I_y = \frac{2}{\Gamma m} \left(\frac{m}{\Omega}\right)^m \frac{\Gamma 2m}{(2A)^m} \frac{2^{-m+0.5}(2m)\sqrt{\pi}}{\Gamma m + 1} \frac{a_1 a_2 h_{fue}}{\sqrt{2A}} \times {}^1F_1\left(m + 0.5; 1.5; \frac{a_1^2 a_2^2 h_{fue}^2}{4A}\right) \ , \qquad (52)$$

where ${}^1F_1(.;.;)$ is the confluent hypergeometric function [25].

We substitute the expression of I_{inner1} in terms of I_x and I_y in Eq. (46) along with the Nakagami-*m* distribution of h_{fue}. Using [29] and [30], the final expression of I_v is obtained. Similarly, we have integral I_u:

$$I_u \cong \int_0^{\infty} [I_{inner2}]\, \mathrm{e}^{\frac{-a_2^2 h_{fue}^2}{2}} f_{h_{fue}}(h_{fue}) \mathrm{d}h_{fue} \ , \qquad (53)$$

where I_{inner2} is:

$$I_{inner2} = \int_0^{\infty} \mathrm{e}^{-\frac{a_1^2 h_{nue}^2}{2}} \mathrm{e}^{-a_1 a_2 h_{nue} h_{fue}} f_{h_{nue}}(h_{nue}) \mathrm{d}h_{nue} \ . \qquad (54)$$

Integral I_{inner2} is solved in the similar manner as Eq. (48) leading to:

$$I_{inner2} = \frac{2}{\Gamma m} \left(\frac{m}{\Omega}\right)^m \frac{\Gamma 2m}{(2A)^m} \mathrm{e}^{\frac{M^2}{8A}} D_{-2m} \left(\frac{M}{\sqrt{2A}}\right) \ , \qquad (55)$$

where $D_v(.)$ is the parabolic cylinder function [25]. Now, we substitute the expression I_{inner2} in Eq. (53) along with the Nakagami-*m* distribution of h_{fue}. Using [30], the final expression of I_u is obtained.

Appendix B

We introduce shaping factor *p* as a parameter which reflects the effect of filtering that is relied upon in the BER analysis of the F-OFDM NOMA signal. In this regard, the value of parameter *p* is chosen depending on the nature of the simulated filter. Since the filter improves SNR of the filtered signal, we define *p* as the ratio between SNR of the filtered OFDM signal and SNR of the unfiltered OFDM signal. Using the simulation parameters given in Section 7, the value of *p* is evaluated as 1.5. All derived expressions consider this shaping factor as a scaling parameter of filtered SNR.

Table 1
BER comparison of F-OFDM NOMA at SNR= 10 dB

Value of p	Simulation BER	Analytical BER
$p = 0.5$	0.0037	0.04
$p = 1$	0.0037	0.011
$p = 1.5$	0.0037	0.00371
$p = 2$	0.0037	0.0012

We also confirm the value of p iteratively, by considering the general AWGN downlink F-OFDM NOMA case of the far user, as shown in Table 1. It is clear that for $p = 1.5$, there is a close match between BER simulations and analytical results.

References

[1] A. Benjebbour *et al.*, "NOMA: From concept to standardization", in *IEEE Conf. on Standards for Commun. and Networking (CSCN)*, Tokyo, 2015, pp. 18–23 (DOI: 10.1109/CSCN.2015.7390414).

[2] D. Tse and P. Viswanath, *Fundamentals of Wireless Communication*. Cambridge University Press, 2005 (ISBN: 9780511807213).

[3] M. Aldababsa, "A tutorial on non-orthogonal multiple access (NOMA) for 5G and beyond", *Wireless Commun. and Mobile Comput.*, vol. 2018, 2018 (DOI: 10.1155/2018/9713450).

[4] S. M. R. Islam, N. Avazov, O. A. Dobre, and K. Kwak, "Power-domain non-orthogonal multiple access (NOMA) in 5G systems: potentials and challenges", in *IEEE Commun. Surveys and Tut.*, vol. 19, no. 2, 2017, pp. 721–742 (DOI: 10.1109/COMST.2016.2621116).

[5] Y. Chen *et al.*, "Toward the standardization of non-orthogonal multiple access for next generation wireless networks", in *IEEE Commun. Mag.*, vol. 56, no. 3, 2018, pp. 19–27 (DOI: 10.1109/MCOM.2018.1700845).

[6] K. Arslan and S. Y. Shin, "Linear precoding techniques for OFDM-based NOMA over frequency-selective fading channels", *IETE J. of Research*, vol. 63, no. 4, 2017, pp. 536–551 (DOI: 10.1080/03772063.2017.1299045).

[7] V. K. Trivedi *et al.*, "Enhanced OFDM-NOMA for next generation wireless communication: A study of PAPR reduction and sensitivity to CFO and estimation errors", *AEU-Int. J. of Electron. and Commun.*, vol. 102, 2019, pp. 9–24 (DOI: 10.1016/j.aeue.2019.01.009).

[8] Y. Cai *et al.*, "Modulation and Multiple Access for 5G Networks", *IEEE Commun. Surveys and Tutorials*, vol. 20, no. 1, pp. 629–646, 2018 (DOI: 10.1109/COMST.2017.2766698).

[9] X. Zhang, M. Jia, L. Chen, J. Ma, and J. Qiu, "Filtered-OFDM – enabler for flexible waveform in the 5th generation cellular networks", in *Proc. IEEE Global Commun. Conf. (GLOBECOM)*, San Diego, 2015, pp. 1–6 (DOI: 10.1109/GLOCOM.2015.7417854).

[10] P. Guan *et al.*, "5G Field Trials: OFDM-based waveforms and mixed numerologies", *IEEE J. on Selected Areas in Commun.*, vol. 35, no. 6, pp. 1234–1243, 2017 (DOI: 10.1109/JSAC.2017.2687718).

[11] F. A. P. de Figueiredo, N. F. T. Aniceto, J. Seki, I. Moerman, and G. Fraidenraich, "Comparing F-OFDM and OFDM performance for MIMO systems considering a 5G scenario", in *Proc. IEEE 2nd 5G World Forum (5GWF)*, Dresden, Germany, 2019, pp. 532–535, (DOI: 10.1109/5GWF.2019.8911702).

[12] J. J. L. Quispe and L. G. P. Meloni, "Pulse shaping filter design for filtered OFDM transceivers", in *Proc. of the 3rd Brazilian Technol. Symp.*, 2019, pp. 131–143 (DOI: 10.1007/978-3-319-93112-8-15).

[13] J. Yli-Kaakinen, T. Levanen, A. Palin, M. Renfors, and M. Valkama, "Generalized fast-convolution-based filtered-OFDM: techniques and application to 5G new radio", *IEEE Transac. on Signal Process.*, vol. 68, pp. 1213–1228, 2020 (DOI: 10.1109/TSP.2020.2971949).

[14] T. B. Deepa, "Performance evaluation of polar coded filtered OFDM for low latency wireless communications", *Wireless Personal Commun.*, 2020 (DOI: 10.1007/s11277-020-07777-2).

[15] K. C. Hu and A. G. Armada, "SINR analysis of OFDM and F-OFDM for machine type communications", in *IEEE 27th Annual Int. Symp. on Personal, Indoor, and Mobile Radio Commun. (PIMRC)*, Valencia, Spain, 2016, pp. 1–6 (DOI: 10.1109/PIMRC.2016.7794702).

[16] S. Wang, J. S. Thompson, and P. M. Grant, "Closed-form expressions for ICI/ISI in filtered OFDM systems for asynchronous 5G uplink", *IEEE Transac. on Commun.*, vol. 65, no. 11, pp. 4886–4898, 2017 (DOI: 10.1109/TCOMM.2017.2698478).

[17] J. Abdoli, M. Jia, and J. Ma, "Filtered OFDM: A new waveform for future wireless systems", in *Proc. IEEE 16th Int. Workshop on Signal Process. Advances in Wireless Commun. (SPAWC)*, 2015, pp. 66–70 (DOI: 10.1109/SPAWC.2015.7227001).

[18] M. Nakagami, "The m-distribution - a general formula of intensity distribution of rapid fading", in *Proc. Statistical Methods in Radio Wave Propag.*, Los Angeles, CA, USA, 1960, pp. 3–36 (DOI: 10.1016/B978-0-08-009306-2.50005-4).

[19] H. Tabassum, M. S. Ali, E. Hossain, M. J. Hossain, and D. I. Kim, "Uplink vs. downlink NOMA in cellular networks: challenges and research directions", in *Proc. IEEE 85th Vehic. Technol. Conf.*, Sydney, 2017, pp. 1–7 (DOI: 10.1109/VTCSpring.2017.8108691).

[20] Y. Neng *et al.*, "Uplink nonorthogonal multiple access technologies toward 5G: A survey", *Wireless Commun. and Mobile Comput.*, 2018 (DOI: 10.1155/2018/6187580).

[21] K. Ferdi and H. Kaya, "BER performances of downlink and uplink NOMA in the presence of SIC errors over fading channels", *IET Commun.*, 2018 (DOI: 10.1049/iet-com.2018.5278).

[22] M. Jain *et al.*, "Performance analysis at far and near user in NOMA based system in presence of SIC error", *AEU-Int. J. of Electronics and Commun.*, 2020, (DOI: 10.1016/j.aeue.2019.152993).

[23] J. Proakis, M. Salehi, and G. Bauch, *Contemporary communication systems using MATLAB*. Nelson Education, 2012 (ISBN: 9780495082514).

[24] M. K. Simon and M. S. Alouini, *Digital Communication Over Fading Channels*. New York: Wiley, 2005 (ISBN: 9780471649533).

[25] I. S. Gradshteyn, I. M. Ryzhik, *Table of integrals, series, and products*. San Diego: Academic Press, 2007 (ISBN: 9780123736376).

[26] N. Kapucu and M. Bilim, "Analysis of analytical capacity for Fisher-Snedecor F fading channels with different transmission schemes", *Electronics Letters*, vol. 55, no. 5, pp. 283–285, 2019 (DOI: 10.1049/el.2018.7813).

[27] Hypergeometric function, *Wolfram mathworld*, 2017 [Online]. Available: https://functions.wolfram.com/PDF/Hypergeometric2F1.pdf

[28] Parabolic cylindrical function, *Wolfram mathworld*, 2017 [Online]. Available: http://functions.wolfram.com/07.41.16.0006.01.

[29] Parabolic cylindrical function *Wolfram mathworld*, 2017 [Online]. Available: https://functions.wolfram.com/PDF/ParabolicCylinderD.pdf

[30] Kummer confluent hypergeometric function *Wolfram mathworld*, 2017 [Online]. Available: http://functions.wolfram.com/07.20.21.0012.01

Shaika Mukhtar received her B.E. and M.Tech. degrees in Electronics and Communication Engineering in 2012 and 2015, respectively. Currently, she is pursuing Ph.D. at the National Institute of Technology, Srinagar. She works as a Senior Research Fellow at the Advanced Communication Lab, NIT Srinagar. Her areas of interest include wireless communication, non-orthogonal multiple access (NOMA), high speed networks and next generation networks. Her research aims at understanding the different aspects of NOMA for future communication networks. She is a student member of IEEE.
E-mail: shaika.mukhtar@yahoo.com
Advanced Communication Lab
Department of Electronics and Communication Engineering
National Institute of Technology Srinagar
Jammu and Kashmir
India

Gh. Rasool Begh received his Ph.D. degree from the National Institute of Technology, Srinagar, India. He works as an Associate Professor at the Department of Electronics and Communication Engineering, NIT Srinagar. His areas of interest include cognitive radios, OFDM, MIMO, cooperative communications, error control coding and security. He is a member of IEEE MTTS.
E-mail: grbegh@nitsri.ac.in
Advanced Communication Lab
Department of Electronics and Communication Engineering
National Institute of Technology Srinagar
Jammu and Kashmir
India